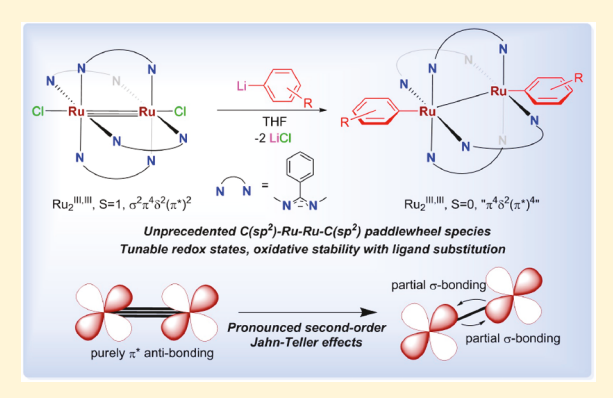
Bisaryl Diruthenium(III) Paddlewheel Complexes: Synthesis and Characterization

Adharsh Raghavan and Tong Ren*

Department of Chemistry, Purdue University, West Lafayette, Indiana 47907, United States

Supporting Information

ABSTRACT: Aryls represent a class of both σ - and π -donating electron-rich axial ligands that is underexplored in the field of metal-metal multiply bonded paddlewheel species. By a decrease in the steric bulk around the diruthenium axial sites and an increase in the basicity of the bridging ligands, the first examples of bisaryl diruthenium(III) paddlewheel complexes have been isolated. Compounds of the form $Ru_2(DMBA)_4Ar_2$ (DMBA = N,N'dimethylbenzamidinate, Ar = C_6H_4 -4- tBu (1), C_6H_5 (2), C_6H_3 -3,5-(OCH₃)₂ (3)) were synthesized via a lithium-halogen exchange reaction between Ru₂(DMBA)₄Cl₂ and excess LiAr and characterized using mass spectrometry, electronic absorption spectroscopy, cyclic and differential pulse voltammetry, and ¹H NMR spectroscopy. The molecular structures of compounds 1-3 were established using single-crystal X-ray diffraction analysis and their electronic



structures (both ground and excited state) analyzed using density functional theory calculations.

INTRODUCTION

Downloaded via PURDUE UNIV on October 14, 2019 at 11:48:37 (UTC). See https://pubs.acs.org/sharingguidelines for options on how to legitimately share published articles.

The discovery of $Ru_2(ap)_4(C_2Ph)$ (ap = 2-anilinopyridinate) by Cotton and Chakravarty has inspired extensive investigation of the organometallic chemistry of di- and triruthenium paddlewheel complexes bearing axial mono- and bisalkynyls, ²⁻¹⁰ and their potential applications as molecular wires in electronic devices have been explored by our laboratory. 11-14 In addition to Ru2 alkynyls, other aspects of di- and triruthenium compounds vigorously pursued in recent years include C-H activation, ¹⁵ aerobic and peroxy oxidation catalysis, ¹⁶⁻²⁰ magnetism, ²¹⁻²³ and devices based on metal strings. 24,25

In comparison to alkynyls, aryls represent a class of σ - and π donating ligands with a stronger electron-donating ability that may lead to Ru, compounds with frontier orbitals energetically distinct from those found in Ru₂ alkynyl compounds. ¹⁰ In this context M2L4(aryl), compounds, whose chemistry remains largely unexplored, are intriguing targets. Currently, there are very few examples of dimetallic aryl complexes either derived from and/or containing a paddlewheel motif (Chart 1). The earliest isolated Ru₂-(aryl)₂ species derived from a paddlewheel motif was reported by Cotton and co-workers.^{26,27} The reaction between Ru₂(PhCONH)₄Cl and PPh₃ resulted in a compound of the formula Ru₂Ph₂(PhCONH)₂[Ph₂POC(Ph)-N₂—a consequence of structural rearrangement of the paddlewheel motif to an edge-sharing bioctahedral motif via the transfer of a Ph group from PPh3 to Ru (C1). The first report of a bis(phenyl) dirhodium(III) paddlewheel complex formed via oxidative arylation of a Rh2(II,III) species came from the Doyle group (C2).28 Since then, their group has

investigated other bisaryl complexes of the form $Rh_2(L)_4(aryl)_2$ (C3). ²⁹⁻³⁴ Interestingly, in these examples, the Rh-Rh bond is absent as a result of a drastic change in the electronic structure of the Rh₂ core to $\pi^4 \delta^2 \pi^{*4} \delta^{*2}$. Until recently, the only example of an $M_2L_4(aryl)_n$ compound with an intact M-M bond and unperturbed paddlewheel came from the laboratories of Bear and Kadish ($\overline{C4}$).³⁵

Recently, we reported the first examples of diruthenium paddlewheel aryls prepared via metathesis with aryllithiums (C5).³⁶ These compounds are remarkably stable under ambient conditions and exhibit rich electrochemical properties by supporting up to four reversible oxidations and one reversible reduction. This electron richness and extended conjugation across the Ru₂ core and aryl ligand prompted us to attempt the isolation of diruthenium aryls in higher oxidation states and to expand their chemistry to include bisaryl species.

Starting from Ru₂(ap)₄Cl, it is indeed possible to synthesize both Ru₂(II,III) and Ru₂(III,III) mono- and bisalkynyl species.^{37,38} However, the steric repulsion between the aryl ligand and the flanking Ph groups of the ap ligand precludes the formation of Ru₂(ap)₄Ar₂ type bisaryl compounds. The ideal bridging ligand for this purpose must provide both a viable Ru₂(III,III) starting point and a sterically less demanding axial coordination site. Out of the few structurally characterized examples of Ru₂^{III,III}L₄X₂-type compounds that exist in the literature, ³⁹ only a small subset of L-type ligands satisfy the above requirements. With this in mind, the highly

Received: August 15, 2019 Published: October 3, 2019

Chart 1. Reported M₂-Aryl Complexes Derived from or Containing a Paddlewheel Motif

$$Ru_{2}(PhCONH)_{4}Cl \xrightarrow{PPh_{3}} Ph_{2}P \xrightarrow{P} Ph_{2}P \xrightarrow{$$

basic and sterically accommodating bidentate ligand DMBA (N_1N' -dimethylbenzamidinate) was chosen. In this contribution are described the synthesis and characterization of three new bisaryl diruthenium complexes of the formula Ru₂(DMBA)₄Ar₂ (Ar = C₆H₄-4- t Bu (1), Ph (2), C₆H₃-3,5-(OCH₃)₂ (3)).

RESULTS AND DISCUSSION

Synthesis. The facile preparation of $Ru_2(DMBA)_4(C_2R)_2$ from $Ru_2(DMBA)_4Cl_2^{40}$ prompted us to examine the synthesis of $Ru_2(DMBA)_4(Ar)_2$ under conditions similar to those for $Ru_2(ap)_4Ar$. The reactions between LiAr (Scheme 1) and $Ru_2(DMBA)_4Cl_2$ were accompanied by a rapid color change from brown to deep red. The consumption of Ru_2 starting material was confirmed by thin-layer chromatography (TLC) and mass spectrometry. Purification of compounds 1-3 was achieved via filtration of the reaction mixture through a triethylamine-deactivated silica plug and elution of a redorange band, followed by recrystallization and washing with cold methanol and hexanes.

The isolated compounds 1-3 are stable in both solution and the solid state under ambient conditions. Like their bis-(alkynyl) counterparts, $Ru_2(DMBA)_4Ar_2$ compounds have a

singlet ground state and thus exhibit diamagnetic ¹H NMR spectra. Further characterization was done using mass spectrometry (ESI-MS), electronic absorption spectroscopy, cyclic (CV) and differential pulse voltammetry (DPV), density functional theory (DFT) calculations, and single-crystal X-ray diffraction studies. Although all three compounds were synthesized using air- and moisture-free techniques, their workups were performed under ambient conditions using solvents that were not rigorously anhydrous. When this is taken into account, satisfactory elemental analyses were obtained for compounds 1–3.

Molecular Structures. Single-crystal X-ray diffraction studies established the molecular structures of compounds 1–3; selected bond lengths are given in Table 1, and the

Table 1. Selected Bond Lengths (Å) and Angles (deg) for Compounds 1-3

	1	2	3
Ru1-Ru2	2.5099(5)	2.4940(3)	2.4928(3)
Ru1-C1	2.078(4)	2.068(1)	2.068(1)
Ru2-Ru1-C1	153.6(1)	152.42(3)	151.23(4)
Ru1-N1	1.99(2)	2.018(1)	2.096(1)
Ru1-N3	2.109(6)	2.0227(9)	2.020(1)
Ru2-N2	2.100(7)	2.1072(9)	2.018(1)
Ru2-N4	2.04(2)	2.1161(8)	2.099(1)

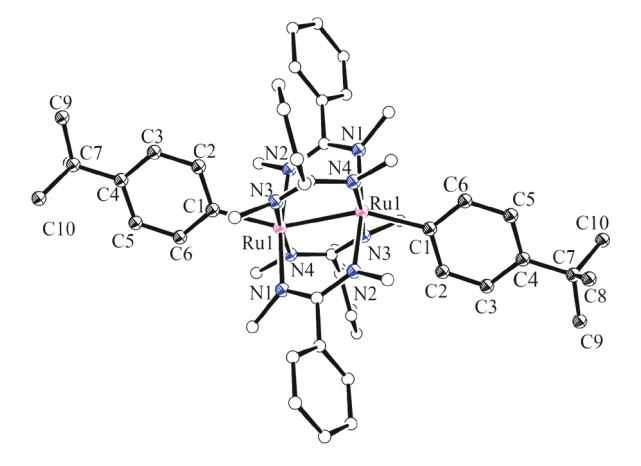


Figure 1. Structural plot of **1** at the 30% probability level. One of the two disordered moieties (A) present in the asymmetric unit was selected. Hydrogens are omitted for clarity.

structures are plotted in Figures 1–3. All three compounds crystallize in the $P\overline{1}$ space group, and each of the individual molecules has an inversion center at the midpoint of the Ru–

Scheme 1. Synthesis of Ru₂(DMBA)₄Ar₂^a

^aNN = N_1N' -dimethylbenzamidinate; R = 4-^tBu (1), H (2), 3,5-(OCH₃)₂ (3).

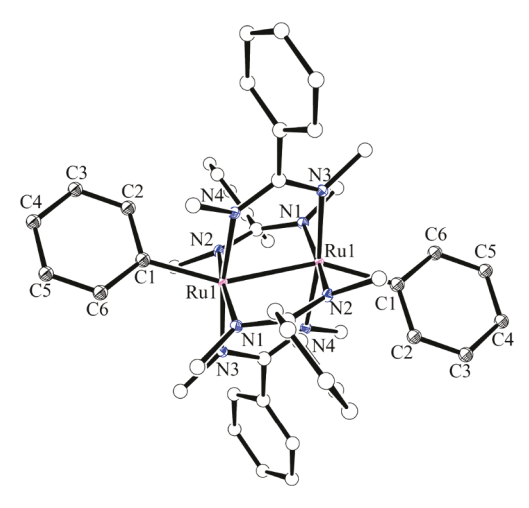


Figure 2. Structural plot of 2 at the 30% probability level. Hydrogens are omitted for clarity.

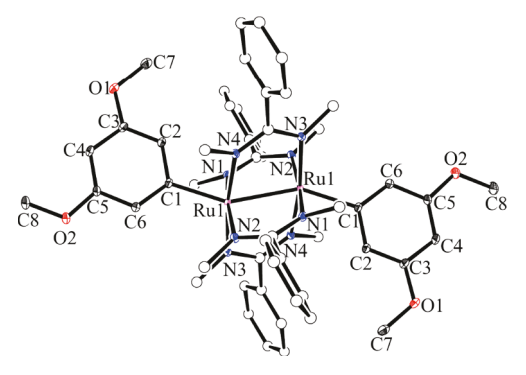


Figure 3. Structural plot of 3 at the 30% probability level. Solvent molecules and hydrogens are omitted for clarity.

Ru bond. The average Ru–Ru bond distance in these compounds is 2.4989(6) Å, significantly longer than that found in Ru₂(DMBA)₄Cl₂ (Ru–Ru = 2.3228(6) Å). The much more strongly σ donating Ar⁻ ligands engage the Ru d_z² orbitals to form strong Ru–C σ bonds, forcing a change in electronic configuration from $\sigma^2\pi^4\delta^2(\pi^*)^2$ to $\pi^4\delta^2(\pi^*)^4$ that is supported by the diamagnetism of 1–3. The absence of a formal σ bond between the metal centers has also been noted by Chisholm and co-workers for bisalkyl ditungsten and dimolybdenum paddlewheel complexes of the form M₂(O₂CR')₄R₂. These formally d³–d³ systems bearing M–M triple bonds have the electronic configuration of $\pi^4\delta^2$.

Indeed, Ru–Ru bond lengths found here are comparable to $Ru_2(DMBA)_4(C \equiv CR)_2$ species (average 2.45 Å) with the same electronic configuration. His effect is also seen in the significant shortening of the Ru–C bond in compounds 1–3 (average 2.071(4) Å) in comparison to those in the recently reported $Ru_2(ap)_4Ar$ species (average 2.21 Å). The Ru– $C(sp^2)$ bond lengths here are slightly longer than the corresponding Ru-C(sp) bond lengths in $Ru_2(DMBA)_4(C \equiv CR)_2$ compounds (average 1.97 Å). The argument here is the same provided for the pairs of $Rh_2(ap)_4(C \equiv CH)$ vs $Rh_2(ap)_4(Ph)^{35}$ and $Ru_2(ap)_4(C \equiv CR)$ vs $Ru_2(ap)_4(Ar)$: (i) an ipso carbon hybridization change from sp to Sp^2 accompanied by an expansion of Sp^2 from 69 to 73 pm⁴³ and (ii) an increase in steric bulk at the axial site. Despite being electronically distinct, the 4- Sp^2 Bu and 3,5- Sp^2 CCH₃ substituents do not significantly influence either

the Ru–Ru or the Ru–C bond lengths because the aryl ligand π orbitals are involved in neither the net single δ bond nor the Ru–C σ bonds.

Compounds 1–3 (Figures 1–3) exhibit a significant distortion from an octahedral geometry at both ruthenium centers. This is reflected in the disparity in Ru-N/Ru'-N' bond lengths and Ru-Ru-N/Ru-Ru-N' bond angles and from the fact that C-Ru-Ru bond angles are significantly less than the ideal 180° (Chart 2). This overall distortion is

Chart 2. Distorted Coordination Geometry Observed in 1– 3^a

$$X \xrightarrow{\stackrel{\nabla}{\underset{\stackrel{\sim}{N'}}{N'}}} \alpha \qquad \beta \xrightarrow{\stackrel{\nabla}{\underset{\stackrel{\sim}{N'}}{N'}}} X$$

 $^{a}\alpha(av) \approx 79.7^{\circ}$, $\beta(av) \approx 95.2^{\circ}$, $\gamma(av) \approx 152^{\circ}$.

attributed to a second-order Jahn—Teller (SOJT) effect, which was first documented and analyzed using a Fenske—Hall type MO analysis for the $Ru_2(DArF)_4(C_2Ph)_2$ series (DArF = diarylformamidinate) by the Ren laboratory 44 and subsequently documented for many of related $Ru_2^{\mbox{\tiny III,III}}L_4X_2$ type complexes. 10 It should be noted that SOJT is probably more common than people realize because of its subtlety. Power and co-workers have noted pronounced SOJT effects in multiply bonded main-group compounds $^{4.5-50}$ and elaborated it in an excellent account in this journal. 51

The extent of structural distortion depends on the nature of the axial substituents. For example, the value of γ in $Ru_2(DMBA)_4X_2$ species where X is Cl⁻, NO_3 ⁻, or BF_4 ⁻ is ca. 180° . So If X is ^{-}C \equiv CR, γ ranges from 161 to 175°, 37,40 and if X is Ar⁻ (compounds 1–3), $\gamma \approx 152^{\circ}$. Structural distortion in $Ru_2^{III,III}L_4(\widehat{C}{\equiv}CR)_2$ complexes has been previously analyzed using DFT calculations, and the results are transferrable here with the major difference being the higher dimensionality of an aryl group in comparison to an alkynyl group.⁵³ Going from a one-dimensional alkynyl to a twodimensional aryl lowers the symmetry of the molecule from D_{4h} to D_{2h} . From an orbital perspective, the two π^* orbitals are no longer degenerate—one is a combination of the π system of aryl and Ru₂(DMBA)₄ whereas the other is purely Ru₂(DMBA)₄-based. In the model compound Ru₂(NHCHNH)₄(C≡CH)₂, lowering the symmetry from D_4 to C_2 is accompanied by a significant stabilization of the $\pi^*(xz)$ orbital while the $\pi^*(yz)$ orbital is more or less unaffected-an effect of HOMO-LUMO mixing. Consequently, the HOMO-LUMO gap is increased and the overall molecular structure is stabilized. A similar effect is seen for 1-3, but to a greater extent presumably because the two $\pi^*(Ru_2)$ orbitals are inherently nondegenerate.

Electrochemistry. Cyclic (CV) and differential pulse voltammetric (DPV) analyses were carried out for compounds 1-3 in CH_2Cl_2 , and three redox events were observed for each of them: namely two oxidations and one reduction (Figure 4 and Table 2). For all three compounds, the first oxidation (B, $Ru_2^{+7/+6}$) is a reversible one-electron event that occurs between -0.41 and -0.54 V (all potentials are reported against $Fc^{+/0}$), while the second oxidation (C) is an irreversible one-electron

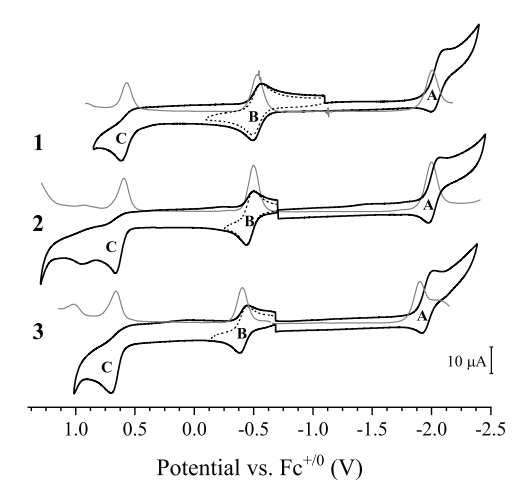


Figure 4. Cyclic (black) and differential pulse (gray) voltammograms of compounds 1-3 (1.0 mM) recorded in 0.10 M $^n\mathrm{Bu}_4\mathrm{NPF}_6$ in $\mathrm{CH}_2\mathrm{Cl}_2$ at a scan rate of 0.10 V/s.

Table 2. Electrode Potentials (V, versus $Fc^{+/0}$) for $Ru_2(DMBA)_4X_2$

X	$E_{1/2}(\mathbf{A})$	$E_{1/2}(\mathbf{B})$	$E_{\rm pa}({f C})^a$
$-C_6H_4-4-^tBu$ (1)	-2.05	-0.53	0.61
$-C_6H_5(2)$	-2.02	-0.47	0.66
$-C_6H_3-3,5-(OCH_3)_2$ (3)	-1.97	-0.42	0.69
$-C \equiv CPh^{40}$	-1.67	-0.056	
-Cl ⁴⁰	-0.89	0.49	
^a Irreversible couple.			

event that occurs between 0.57 and 0.66 V. Unlike more electron-rich aryls such as C_6H_4 -4-NR₂, those of compounds 1–3 are not necessarily suited to stabilize a cationic charge upon oxidation. Thus, the irreversible nature of C suggests that it might be aryl ligand based. The only reduction event observed for all three compounds (A, $Ru_2^{+6/+5}$) is initially quasi-reversible but becomes irreversible upon repeated scans. Quasi-reversibility is restored upon polishing the working electrode between scans. Such a behavior suggests ligand dissociation of the axial aryls or of the DMBA ligands.

Aryls are much stronger electron donors than alkynyls, and this is reflected in the ca. 0.44 V cathodic shift of the reduction potential of event B (Ru2 $^{+7/+6}$) upon going from Ru2(DMBA)4(C \equiv CPh)2 to Ru2(DMBA)4(Ph)2. This ability of compounds 1–3 to undergo oxidation at low potentials is noteworthy. While compounds 2 and 3 are stable as Ru2 $^{\text{III,III}}$ complexes under ambient conditions, 1 was isolated with a minor paramagnetic impurity. This is seen from the fact that the 1 H NMR peaks (in CDCl3) of 2 and 3 are sharp and well-defined, whereas those of 1 are ill-defined and slightly broadened (Figures S5–S7). In order to obtain a clean diamagnetic spectrum of 1, a slight excess of NaBH4 was added to the NMR tube (Figure S5b). Thus, even a weakly electron donating substituent such as p-Bu can result in the facile o x i d a t i o n o f R u $_2$ $_{1111,111}^{1111}$ (D M B A) $_4$ (A r) $_2$ to [Ru2 $_2$ $_{1111,111}^{1111}$ (D M B A) $_4$ (A r) $_2$ to [Ru2 $_2$ $_{1111,111}^{1111}$ (D M B A) $_4$ (A r) $_2$ to [Ru2 $_2$ $_{1111,111}^{1111}$ (D M B A) $_4$ (A r) $_2$] $_1$.

Electronic Absorption Spectroscopy. Figure 5 shows the vis—NIR absorption spectra of compounds 1—3 in THF. The most intense transitions occur at 390 and 490 nm for all three complexes—the latter being the color-producing band, since they all appear to take on a similar shade of red in solution. The spectroscopic features seen here are reminiscent

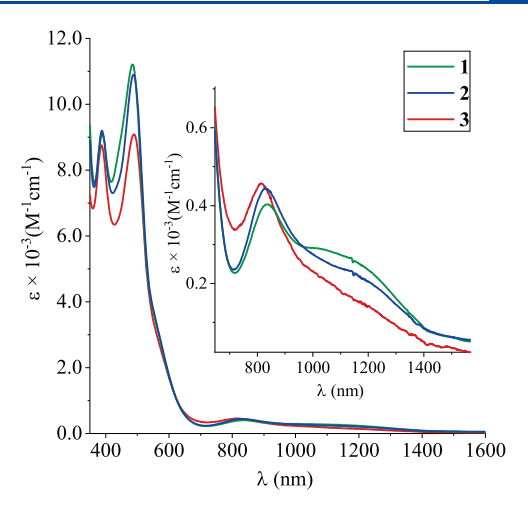


Figure 5. Vis-NIR spectra of compounds 1-3 in THF.

of those for $Ru_2(DMBA)_4(C \equiv CR)_2$ complexes with a few differences.

The two weakly absorbing transitions seen above 800 nm for compounds 1-3 are different from the one intense absorption at ca. 860 nm for $Ru_2(DMBA)_4(C \equiv CR)_2$ species, which can be explained by the loss of degeneracy of the frontier $\pi^*(Ru_2)$ orbitals resulting from the two-dimensional aryl ligands. One of the d orbitals $(d_{xz}$ or $d_{yz})$ is perpendicular to the plane of Ar-, while the other is coplanar and consequently is not affected by it. The lowest energy absorption at ca. 1100 nm likely belongs to the HOMO $(\pi^*) \to \text{LUMO }(\delta^*)$ transition, as is evident from the slight blue shift upon going from compound 1 to 3: i.e. from electron-donating 4-^tBu to electron-withdrawing 3,5-(OCH₃)₂. The low intensity of the peaks suggests that they are mainly metal based and that the dependence on the aryl ligand is likely due to inductive effects. In contrast, the intensities of the absorptions at ca. 490 and 390 nm and, to a certain extent, the shoulder peak at ca. 570 nm suggest that some sort of charge transfer process is at play, either metal to ligand (MLCT) or ligand to metal (LMCT). To better characterize the nature of these electronic transitions, time-dependent DFT (TD-DFT) calculations were performed on compound 2, the results of which are discussed below.

Density Functional Theory (DFT) Calculations. To understand the ground state electronic structure of these complexes, the molecular orbitals (MOs) of Ru₂(DMBA)₄Ph₂ were computed using spin-restricted DFT. The optimized geometry 2' was based on the crystal structure of compound 2. Figure 6 shows the frontier MOs of 2' based on calculations done using the B3LYP functional, 54-57 with the def2-TZVP/def2-SVP basis sets, 58,59 including Grimme's dispersion correction (D3).60 The optimized geometric parameters are in agreement with the crystallographically determined structure of 2. Details of the computational methods are provided in the Supporting Information.

As expected, the HOMO is a $\pi^*(Ru_2/Ar)$ orbital with contributions from both the diruthenium core and the aryl ligand, whereas the LUMO is a $\delta^*(Ru_2)$ orbital with additional contribution from the nonbonding $\pi(N-C-N)$ of the DMBA ligands. Consistent with the energy lowering of one of the two π^* orbitals due to the SOJT effects discussed above and with the fact that aryls are good π -donor ligands, HOMO-1 lacks π^* character; in its place is the high-lying $\pi(Ru_2/Ar)$ orbital.

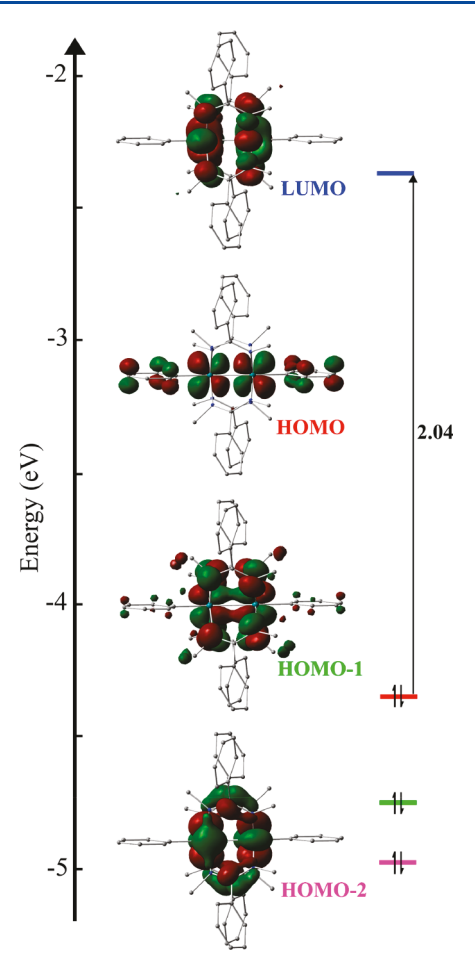


Figure 6. Molecular orbital diagram of 2' obtained from DFT calculations, represented at lisovalue = 0.03.

HOMO-2 is the familiar $\delta(\mathrm{Ru_2})/\pi(\mathrm{Ru-N})$ orbital, devoid of any contribution from the axial ligand. Hence, across the series 1–3 the δ – δ * gap is expected to remain invariant.

The effect of the large deviation from linearity of the Ru–Ru–C bond on the electronic structure is readily seen from the HOMO-4 orbital (Figure 7), a $\pi^*(\text{Ru-Ru})$ orbital that has gained some σ -bonding character. As mentioned previously, this phenomenon has been observed with the model compound Ru₂(NHCHNH)₄(C \equiv CH)₂. Thus, while the overall ground state d-electron configuration for Ru₂ can be

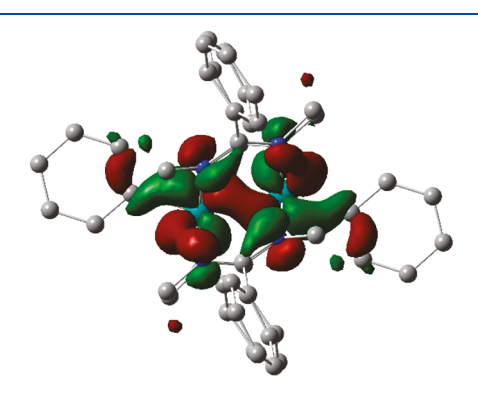


Figure 7. HOMO-4 for the optimized structure 2', a π^* (Ru–Ru) orbital with σ-bonding character.

simplified as $\pi^4 \delta^2(\pi^*)^4$, the actual ordering of the MOs is certainly more complex, namely $(\pi^* + \sigma)^2 \pi^2 \delta^2 \pi^2 (\pi^*)^2$.

In addition to ground-state calculations, TD-DFT analysis was carried out on the optimized structure 2' in order to better understand the nature of its electronic excited states. Table S3 in the Supporting Information gives the most significant transitions calculated by TD-DFT, and Table 3 below depicts the MO diagrams of the natural transition orbitals (NTOs)

Table 3. Natural Transition Orbitals Derived from TD-DFT Calculations a

Excited	$\bar{\nu}$ (cm ⁻¹)	NTO1	NTO2
state			
1	6331.45	*# %	
4	12958.87		
6	17858.87 (major)		1
6	17858.87 (minor)	CASON CONTRACTOR	cielos.
7	20500.80 (major)		
7	20500.80 (minor)		•••
9	21390.32		
10	21892.74 (major)	2-12 A 2-12	
10	21892.74 (minor)		
18	27436.29 (major)	CHARL	igni
18	27436.29 (minor)		

^aTransitions are noted as NTO1 \rightarrow NTO2.

calculated on the basis of each of the excited states.⁶¹ Figure 8 shows the deconvoluted electronic absorption spectrum of 2 in THF, and Figure S4 shows the absorption spectrum of 2' simulated from TD-DFT results.

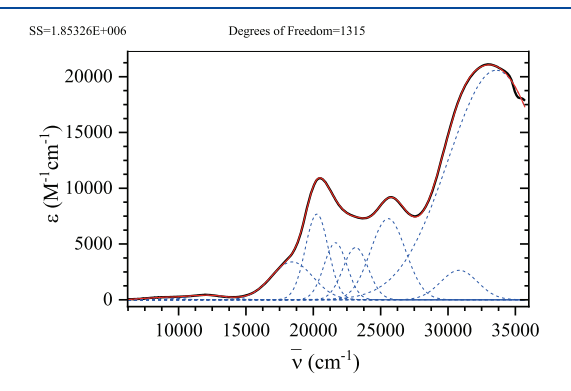


Figure 8. Experimental curve (black), fit peaks (blue, dashed) and cumulative fit curve (red) obtained from Gaussian deconvolution of the electronic absorption spectrum of **2** in THF.

While quantitative differences between experiment and theory do exist, TD-DFT is indeed able to qualitatively illustrate the natures of the most important absorptions seen in the vis-NIR spectrum of 2. The two low-intensity peaks below 13000 cm⁻¹ are both expected to be d-d transitions with minor contributions from both the axial and equatorial ligand. Accordingly, TD-DFT predicts the lowest energy absorption feature observed at ca. 8700 cm $^{-1}$ to belong to the HOMO \rightarrow LUMO transition $(\pi^*(Ru_2/Ar) \rightarrow \delta^*(Ru_2)/p(N))$. The second low-intensity peak calculated at ca. 13000 cm⁻¹ also agrees with the measured value of ca. 12000 cm⁻¹ and is predicted to be $\pi^*(Ru_2) \rightarrow \delta^*(Ru_2)/p(N)$ in nature. This $\pi^*(Ru_2)$ orbital is coplanar with the aryl ligand and hence unaffected by its π system. Thus, while the transition at 8700 cm⁻¹ is dependent on the nature of the axial substituent, as can be seen from Figure 5, the latter peak is invariant at ca. 12000 cm⁻¹. The shoulder peak that appears at ca. 18000 cm⁻¹ agrees well with the predicted value of 17858 cm⁻¹. NTO analysis reveals that this transition has two components: namely, $\delta(Ru_2)/\pi(NCN) \rightarrow \delta^*(Ru_2)/p(N)$ (major) and $\pi(Ru_2) \rightarrow$ $\sigma^*(Ru-C)$ (minor).

The most intense absorption features observed between $19000 \text{ and } 27000 \text{ cm}^{-1} \text{ can be deconvoluted into four peaks of}$ comparable intensities (Figure 8). Qualitatively, four similar transitions of comparable oscillator strengths are indeed predicted by TD-DFT, which can be grouped into two categories. The first category consists of the experimentally observed (and calculated via Gaussian deconvolution) peaks at 20264, 21649, and 23145 cm⁻¹. These are in good agreement with the predicted transitions at 20500, 21390, and 21890 cm⁻¹, respectively. NTO analysis suggests that the two major contributors for this category are ligand to metal charge transfer $p(N) \rightarrow \delta^*(Ru_2)$ and $\pi(Ru_2) \rightarrow \sigma^*(Ru-C)$. The second category contains the fourth transition measured at 25560 cm⁻¹, the predicted value for which is ca. 27400 cm⁻¹. The major contribution for this peak is predicted to come from a $\pi(Ru_2) \to \sigma^*(Ru-C)$ transition, both of which have metal (major) and aryl ligand (minor) characters.

CONCLUSION

Reported herein are the first examples of M2 bisaryl paddlewheel complexes with intact M-M bonds. The strong σ -donating ability of the aryl ligands forces a change in electronic configuration from $\sigma^2 \pi^4 \delta^2 (\pi^*)^2$ (S = 1) in $Ru_{2}(DMBA)_{a}Cl_{2}$ to " $\pi^{4}\delta^{2}(\pi^{*})^{4}$ " (S = 0) in $Ru_{2}(DMBA)_{a}Ar_{2}$ (compounds 1-3), while their strong π -donating ability is evident from both electronic absorption spectroscopy and DFT calculations. The superior electron-donating ability of the aryls in comparison to alkynyls is evident from the ca. 400-500 mV cathodic shift of $E(Ru_2^{+7/+6})$, the first oxidation potential, from Ru₂(DMBA)₄(C\equiv CAr)₂ to Ru₂(DMBA)₄Ar₂. Computational modeling of the electronic structure of Ru₂(DMBA)₄Ar₂-type complexes has been achieved through both ground-state DFT and TD-DFT analyses of 2', which indicate significant mixing of the metal and ligand (both axial and equatorial) orbitals. Additionally, DFT also sheds light on the effect of SOJT distortions on the $\pi^*(Ru-Ru)$ orbital, which gains significant σ character. Overall, for M_2 paddlewheel species, aryls represent a new class of both σ and π -donating electron-rich axial ligands, and the intriguing chemistry of the Ru-Ru-C(sp²) motif is being further explored in our laboratory.

EXPERIMENTAL SECTION

General Considerations. Ru₂(DMBA)₄Cl₂ was prepared using a literature method. 40 BuLi (2.5 and 1.6 M in hexanes) was purchased from Sigma-Aldrich. Aryl halides were purchased from commercial sources and used as received. Tetrahydrofuran was freshly distilled over sodium/benzophenone, while dichloromethane was freshly distilled over CaH2 prior to use. All reactions were performed under a dry N2 atmosphere with standard Schlenk techniques implemented unless otherwise noted. All reagents were thoroughly dried and degassed prior to lithiation. UV-vis-NIR spectra were obtained with a JASCO V-670 spectrophotometer in THF solutions. ¹H NMR spectra were recorded on a Varian Mercury 300 spectrometer operating at 299.953 MHz. Cyclic and differential pulse voltammograms were recorded in 0.1 M ["Bu₄N][PF₆] solution (CH₂Cl₂, Ar degassed) on a CHI620A voltammetric analyzer with a glassy-carbon working electrode (diameter 3 mm), a Pt-wire auxiliary electrode, and a Ag/AgCl quasi-reference electrode. The concentration of Ru₂ species was always ca. 1.0 mM. The Fc^{+/0} couple was observed at ca. 0.51 ± 0.064 V under the noted experimental conditions. Elemental analyses were performed by Atlantic Microlab

Synthesis of $Ru_2(DMBA)_4(C_6H_4-4-{}^tBu)_2$ (1). To a THF (10 mL) solution of 1-bromo-4-tert-butylbenzene (0.60 mL, 3.5 mmol) at -78 °C was added, dropwise, 2.2 mL of "BuLi (1.6 M in hexanes). The aryllithium solution was slowly warmed to ca. 0 °C and transferred via cannula to Ru₂(DMBA)₄Cl₂ (75 mg, 0.09 mmol) dissolved in 20 mL of THF. The solution immediately changed from brown to deep red. After it was stirred for ca. 30 min under dinitrogen, the solution was concentrated and filtered through a Celite plug. The filtrate was collected, solvent removed, and the product recrystallized twice from THF/MeOH and CH₂Cl₂/hexanes at −20 °C. The precipitate was rinsed with *n*-pentane and dried to afford a red-brown solid (25 mg, 27% yield). Crystals suitable for X-ray diffraction analysis were grown by layering hexanes over a solution of 1 in CHCl3. Data for 1 are as follows. Anal. Found (calcd) for C₅₇H₇₄Cl₂N₈ORu₂ (1•CH₂Cl₂•H₂O): C, 58.77 (59.00); H, 6.22 (6.43); N, 9.43 (9.66). ESI-MS (m/z) [1⁺]: 1057.4. UV-vis (in THF) λ , nm (ε , M⁻¹ cm⁻¹): 388 (9100), 484 (11000), 575 (sh, ~2800), 836 (400), 1132 (270). Electrochemistry (CH₂Cl₂, vs Fc^{+/0}), $E_{1/2}$ /V, ΔE_p /mV, $i_{forward}$ / $i_{backward}$: 0.61 (E_{pa}), irrev; -0.53, 77, 1.0; -2.1, ~2.1. ¹H NMR (CDCl₃, 25 °C) δ, ppm: 1.27 (s, 18H, p-C(CH₃)₃), 3.02 (br, 24H, DMBA N-(CH₃)₂), 6.87–7.12 (br,

12H, DMBA o-CH and aryl o-/m-CH), 7.28-7.54 (m, 16H, DMBA m- and p-CH, and aryl m-/o-CH).

Synthesis of Ru₂(DMBA)₄Ph₂ (2). To a THF (15 mL) solution of bromobenzene (0.15 mL, 1.4 mmol) at -78 °C was added, dropwise, 0.6 mL of "BuLi (2.5 M in hexanes). The aryllithium solution was slowly warmed to ca. 0 °C and transferred via cannula to Ru₂(DMBA)₄Cl₂ (150 mg, 0.17 mmol) dissolved in 20 mL of THF. The solution immediately changed from brown to deep red. After it was stirred for ca. 30 min under dinitrogen, the solution was concentrated and filtered through a deactivated (with triethylamine) silica plug. The red-brown filtrate was collected, solvent removed, and a red microcrystalline solid recrystallized from CH2Cl2/hexanes at -20 °C. The precipitate was rinsed with cold methanol and *n*-pentane and dried to afford a red microcrystalline solid (65 mg, 40% yield). Crystals suitable for X-ray diffraction analysis were grown by layering hexanes over a solution of 2 in CH₂Cl₂. Data for 2 are as follows. Anal. Found (calcd) for C₅₀H₅₈Cl₄N₈Ru₂ (2·2CH₂Cl₂): C, 54.28 (53.86); H, 5.35 (5.24); N, 10.18 (10.05). ESI-MS (m/z) [2⁺]: 945.7. UV-vis (in THF) λ , nm (ε , M⁻¹ cm⁻¹): 388 (9200), 487 (11000), 580 (sh, ~2500), 830 (440), 1132 (220). Electrochemistry (CH₂Cl₂, vs Fc^{+/0}), $E_{1/2}$ /V, $\Delta E_{\rm p}$ /mV, $i_{\rm forward}$ / $i_{\rm backward}$: 0.66 ($E_{\rm pa}$), irrev; -0.47, 60, 1.1; -2.0, 100, 1.4. ¹H NMR (CDCl₃, 25 °C) δ, ppm: 3.05 (s, 24H, DMBA N-(CH₃)₂), 6.61 (br, 2H, aryl p-CH), 6.80 (t, 4H, aryl m-CH), 6.99 (d, 8H, DMBA o-CH), 7.12 (br, 4H, aryl o-CH), 7.30-7.45 (m, 12H, DMBA m- and p-CH).

Synthesis of $Ru_2(DMBA)_4(C_6H_3-3,5-(OCH_3)_2)_2$ (3). To a THF (15 mL) solution of 1-bromo-3,5-dimethoxybenzene (375 mg, 1.7 mmol) at -78 °C was added, dropwise, 0.7 mL of "BuLi (2.5 M in hexanes). The aryllithium solution was slowly warmed to ca. 0 °C and transferred via cannula to Ru₂(DMBA)₄Cl₂ (100 mg, 0.12 mmol) dissolved in 15 mL of THF. The solution immediately changed from brown to deep red. After it was stirred for ca. 30 min under dinitrogen, the solution was concentrated and filtered through a Celite plug. The red-brown filtrate was collected, solvent removed, and a red-brown solid product twice recrystallized from CH2Cl2/hexanes at -20 °C. The microcrystalline precipitate was rinsed with cold methanol and n-pentane and dried (56 mg, 45% yield). Crystals suitable for X-ray diffraction analysis were grown by layering hexanes over a solution of 3 in CH2Cl2. Data for 3 are as follows. Anal. Found (calcd) for $C_{54.5}H_{67}Cl_5N_8O_5Ru_2(3\cdot2.5CH_2Cl_2)$: C, 51.41 (51.24); H, 5.17 (5.29); N, 8.89 (8.77). ESI-MS (m/z) [3⁺]: 1065.3. UV-vis (in THF) λ , nm (ε , M⁻¹ cm⁻¹): 387 (8700), 489 (9100), 570 (sh, ~2700), 814 (460), 1100 (180). Electrochemistry (CH₂Cl₂, vs Fc^{+/0}), $E_{1/2}/V$, $\Delta E_{\rm p}/{\rm mV}$, $i_{\rm forward}/i_{\rm backward}$: 0.69 ($E_{\rm pa}$), irrev; -0.42, 64, 0.99; -1.9, 104, 2.1. ¹H NMR (CDCl₃, 25 °C) δ , ppm: 3.09 (s, 24H, DMBA N- $(CH_3)_2$), 3.70 (s, 12H, OCH₃), 5.84 (s, 2H, aryl p-CH), 6.33 (s, 4H, aryl o-CH), 6.96 (d, 8H, DMBA o-CH), 7.31-7.44 (m, 12H, DMBA m- and p-CH).

X-ray Crystallographic Analysis. Single-crystal X-ray diffraction data for compounds 1–3 at 150 K were collected on a Bruker AXS D8 Quest CMOS diffractometer using Mo K α radiation (λ = 0.71073 Å). Data were collected and processed using APEX3,⁶² and the structures were solved using the SHELXTL suite of programs^{63,64} and refined using Shelxl2016.^{65,66}

ASSOCIATED CONTENT

S Supporting Information

The Supporting Information is available free of charge on the ACS Publications website at DOI: 10.1021/acs.organomet.9b00555.

Computational methods and results, including DFT-optimized structures, TD-DFT results, Gaussian deconvolution fitting results, ¹H NMR spectra, and crystallographic details (PDF)

Cartesian coordinates (PDF)

Accession Codes

CCDC 1947221–1947223 contain the supplementary crystallographic data for this paper. These data can be obtained free of charge via www.ccdc.cam.ac.uk/data_request/cif, or by emailing data_request/cif, or by contacting The Cambridge Crystallographic Data Centre, 12 Union Road, Cambridge CB2 1EZ, UK; fax: +44 1223 336033.

AUTHOR INFORMATION

Corresponding Author

*E-mail for T.R.: tren@purdue.edu.

ORCID ®

Tong Ren: 0000-0002-1148-0746

Notes

The authors declare no competing financial interest.

ACKNOWLEDGMENTS

We thank the National Science Foundation for generously supporting this work (CHE 1764347 for research and CHE 1625543 for X-ray diffractometers). We also thank Dr. Pradeep Kumar Gurunathan and Mr. Alireza Karbakhsh Ravari for helpful discussions on DFT calculations.

REFERENCES

- (1) Chakravarty, A. R.; Cotton, F. A. A New Diruthenium(II, III) Compound, Ru2(CCPh)(PhNpy)4.2CH2Cl2, with an Axial Acetylide Ligand. *Inorg. Chim. Acta* **1986**, *113*, 19–26.
- (2) Bear, J. L.; Han, B.; Huang, S. Molecular Structure and Electrochemistry of Ru2(dpf)4(CCPh)2: A Novel Ru(III)-Ru(III) Dimer. J. Am. Chem. Soc. 1993, 115, 1175–1177.
- (3) Li, Y.; Han, B.; Kadish, K. M.; Bear, J. L. A Novel Diamagnetic Diruthenium(III) Complex Bridged by Four Unsymmetrical Carboxylate-Type Ligands. *Inorg. Chem.* **1993**, *32*, 4175–4176.
- (4) Bear, J. L.; Han, B.; Huang, S.; Kadish, K. M. Effect of Axial Ligands on the Oxidation State, Structure, and Electronic Configuration of Diruthenium Complexes. *Inorg. Chem.* **1996**, 35, 3012–3021.
- (5) Bear, J. L.; Han, B.; Wu, Z.; Caemelbecke, E. V.; Kadish, K. M. Synthesis, Electrochemistry, and Spectroscopic Characterization of Bis-dirhodium Complexes Linked by Axial Ligands. *Inorg. Chem.* **2001**, *40*, 2275–2281.
- (6) Kuo, C.; Chang, J.; Yeh, C.; Lee, G.; Wang, C.; Peng, S. Synthesis, structures, magnetism and electrochemical properties of triruthenium-acetylide complexes. *Dalton Trans* **2005**, 3696–3701.
- (7) Zuo, J.-L.; Herdtweck, E.; Biani, F. F. d.; Santos, A. M.; Kühn, F. E. Ruthenium(II) alkynyl-hydride and ruthenium(II) bis(-pyridylacetylide) as ligands and linkers for metal—metal-bonded complexes. *New J. Chem.* **2002**, *26*, 889—894.
- (8) Zuo, J.-L.; Herdtweck, E.; Kühn, F. E. Diruthenium s-alkynyl complexes as potential building blocks for heterometallic molecular rods. *J. Chem. Soc. Dalt. Trans.* **2002**, 1244–1246.
- (9) Zuo, J.-L.; Biani, F. F. d.; Santos, A. M.; Köhler, K.; Kühn, F. E. 4-Ethynylpyridine as a Bridging Moiety in Mixed Rh/Re Complexes. *Eur. J. Inorg. Chem.* **2003**, 2003, 449–452.
- (10) Ren, T. Diruthenium ó-alkynyl compounds: A new class of conjugated organometallics. *Organometallics* **2005**, *24*, 4854–4870.
- (11) Blum, A. S.; Ren, T.; Parish, D. A.; Trammell, S. A.; Moore, M. H.; Kushmerick, J. G.; Xu, G.-L.; Deschamps, J. R.; Pollack, S. K.; Shashidhar, R. $Ru_2(ap)_4((-oligo(phenyleneethynyl)))$ Molecular Wires: Synthesis and Electronic Characterization. *J. Am. Chem. Soc.* **2005**, *127*, 10010–10011.
- (12) Mahapatro, A. K.; Ying, J.; Ren, T.; Janes, D. B. Electronic Transport through Ruthenium Based Redox-Active Molecules in Metal-Molecule-Metal Nanogap Junctions. *Nano Lett.* **2008**, *8*, 2131–2136.

(13) Pookpanratana, S.; Zhu, H.; Bittle, E. G.; Natoli, S. N.; Ren, T.; Richter, C. A.; Li, Q.; Hacker, C. A. Non-volatile memory devices with redox-active diruthenium molecular compound. *J. Phys.: Condens. Matter* **2016**, *28*, 094009.

- (14) Zhu, H.; Pookpanratana, S. J.; Bonevich, J. E.; Natoli, S. N.; Hacker, C. A.; Ren, T.; Suehle, J. S.; Richter, C. A.; Li, Q. Redox-Active Molecular Nanowire Flash Memory for High-Endurance and High-Density Nonvolatile Memory Applications. *ACS Appl. Mater. Interfaces* **2015**, *7*, 27306–27313.
- (15) Musch Long, A. K.; Yu, R. P.; Timmer, G. H.; Berry, J. F. Aryl C-H Bond Amination by an Electrophilic Diruthenium Nitride. *J. Am. Chem. Soc.* **2010**, *132*, 12228–12230.
- (16) Barker, J. E.; Ren, T. Diruthenium(II,III) Bis(tetramethyl-1,3-benzenedipropionate) As A Novel Catalyst for tert-Butyl Hydroperoxide Oxygenation. *Inorg. Chem.* **2008**, *47*, 2264–2266.
- (17) Lee, H. B.; Ren, T. Aerobic Oxygenation of Organic Sulfides using Diruthenium Activators. *Inorg. Chim. Acta* **2009**, *362*, 1467–1470
- (18) Villalobos, L.; Cao, Z.; Fanwick, P. E.; Ren, T. Diruthenium-(II,III) tetramidates as a new class of oxygenation catalysts. *Dalton Trans* **2012**, *41*, 644–650.
- (19) Villalobos, L.; Paredes, J. E. B.; Cao, Z.; Ren, T. TBHP Oxygenation of Organic Sulfides Catalyzed by Diruthenium(II,III) Tetracarboxylates. *Inorg. Chem.* **2013**, *52*, 12545.
- (20) Corcos, A. R.; Pap, J. S.; Yang, T.; Berry, J. F. A Synthetic Oxygen Atom Transfer Photocycle from a Diruthenium Oxyanion Complex. J. Am. Chem. Soc. 2016, 138, 10032–10040.
- (21) Barral, M. C.; Herrero, S.; Jiménez-Aparicio, R.; Torres, M. R.; Urbanos, F. A. A Spin-Admixed Ruthenium Complex. *Angew. Chem., Int. Ed.* **2005**, *44*, 305–307.
- (22) Barral, M. C.; Gallo, T.; Herrero, S.; Jiménez-Aparicio, R.; Torres, M. R.; Urbanos, F. A. Equatorially Connected Diruthenium-(II,III) Units toward Paramagnetic Supramolecular Structures with Singular Magnetic Properties. *Inorg. Chem.* **2006**, *45*, 3639–3647.
- (23) Cortijo, M.; González-Prieto, R.; Herrero, S.; Priego, J. L.; Jiménez-Aparicio, R. The use of amidinate ligands in paddlewheel diruthenium chemistry. *Coord. Chem. Rev.* **2019**, *400*, 213040.
- (24) Shih, K. N.; Huang, M. J.; Lu, H. C.; Fu, M. D.; Kuo, C. K.; Huang, G. C.; Lee, G. H.; Chen, C. H.; Peng, S. M. On the tuning of electric conductance of extended metal atom chains via axial ligands for Ru-3(mu(3)-dpa)(4)(X)(2) (0/+) (X = NCS-, CN-). Chem. Commun. 2010, 46, 1338–1340.
- (25) Tsai, C. S.; Liu, I. P. C.; Tien, F. W.; Lee, G. H.; Yeh, C. Y.; Chen, C. H.; Peng, S. M. A novel triruthenium metal string complex with naphthylridylamide ligand: Synthesis, structure, magnetism, and molecular conductance. *Inorg. Chem. Commun.* **2013**, *38*, 152–155.
- (26) Chakravarty, A. R.; Cotton, F. A.; Tocher, D. A. Displacive Transfer of a Phenyl Group from Triphenylphosphine to a Metal Atom: Synthesis and Molecular Structure of Ru₂Ph₂(PhCONH)₂[Ph₂POC(Ph)N]₂. J. Am. Chem. Soc. 1984, 106, 6409-6413.
- (27) Chakravarty, A. R.; Cotton, F. A. The Aryl Group Transfer Process From a Triarylphosphine to a Chlorotetrakis(Amidato)-Diruthenium(II,III) Species Syntheses and Molecular-Structures of $Ru_2(R)_2(R'CONH)_2[R_2POC(R')N]_2$ ($R=C_6H_5$, $R'=3,5-(OCH_3)_2C_6H_3-R=para-C_6H_4CH_3$, $R'=C_6H_5$). Inorg. Chem. 1985, 24, 3584–3589.
- (28) Nichols, J. M.; Wolf, J.; Zavalij, P.; Varughese, B.; Doyle, M. P. Bis(phenyl)dirhodium(III) Caprolactamate: A Dinuclear Paddlewheel Complex with No Metal-Metal Bond. *J. Am. Chem. Soc.* **2007**, *129*, 3504–3505.
- (29) Xie, J. H.; Nichols, J. M.; Lubek, C.; Doyle, M. P. Synthesis of bis(ó-aryl)dihodium(III) caprolactamates by oxidative arylation with arylboronic acids. *Chem. Commun.* **2008**, 2671–2673.
- (30) Wolf, J.; Poli, R.; Xie, J. H.; Nichols, J.; Xi, B.; Zavalij, P.; Doyle, M. P. Removal of metal-metal bonding in a dimetallic paddlewheel complex: Molecular and electronic structure of bis(phenyl) dirhodium(III) carboxamidate compounds. *Organometallics* **2008**, 27, 5836–5845.

(31) Xie, J. H.; Zhou, L.; Lubek, C.; Doyle, M. P. Hetero-bis(ó-aryl)dirhodium(III) caprolactamates. Electronic communication between aryl groups through dirhodium(III). *J. Chem. Soc. - Dalt. Trans.* **2009**, 2871–2877.

- (32) Xie, J. H.; Zhou, L.; Zavalij, P.; Doyle, M. P.; Sun, Y.; Liu, Y.; Sun, H. Conformational isomers of extraordinary stability: Carboxamidate-bridged dimetalloorganic compounds. *Chem. Commun.* **2009**, 3005–3007.
- (33) Doyle, M. P.; Shabashov, D.; Zhou, L.; Zavalij, P. Y.; Welch, C.; Pirzada, Z. Does an axial propeller shape on a dirhodium(III,III) core affect equatorial ligand chirality? *Organometallics* **2011**, *30*, 3619–3627.
- (34) Angelone, D.; Draksharapu, A.; Browne, W. R.; Choudhuri, M. M. R.; Crutchley, R. J.; Xu, X. C.; Xu, X. F.; Doyle, M. P. Dinuclear compounds without a metal-metal bond. Dirhodium(III,III)-carboxamidates. *Inorg. Chim. Acta* **2015**, 424, 235–240.
- (35) Bear, J. L.; Han, B.; Li, Y.; Ngubane, S.; Van Caemelbecke, E.; Kadish, K. M. Synthesis, spectroscopic properties and electrochemistry of $Rh_2(ap)_4(R)$ where $R = CH_3$ or C_6H_5 and ap = 2-anilinopyridinate anion. *Polyhedron* **2009**, 28, 1551–1555.
- (36) Raghavan, A.; Mash, B. L.; Ren, T. Forging Ru- $C_{\rm sp}2$ Bonds in Paddlewheel Complexes Using the Lithium-Halogen Exchange Reaction. *Inorg. Chem.* **2019**, 58, 2618–2626.
- (37) Ren, T. Dissymmetrical trans- Ethynyl-Butadiynyl Adducts on a Diruthenium Core: Synthesis, Characterization, and Selective Deprotection. *Organometallics* **2002**, *21*, 732–738.
- (38) Xu, G.; Ren, T. Ru-ó-butadiynyl Complexes of the Tetraanilinopyridinatodiruthenium Core: Formation of a Bis-adduct. *Organometallics* **2001**, *20*, 2400–2404.
- (39) Angaridis, P. In *Multiple Bonds between Metal Atoms*; 3rd ed.; Cotton, F. A., Murillo, C. A., Walton, R. A., Eds.; Springer Science and Business Media: New York, 2005.
- (40) Xu, G.; Campana, C.; Ren, T. Tetrakis(N,N'-dimethylbenzamidinato)diruthenium(III) Compounds Bearing Axial Chloro and Alkynyl Ligands: A New Family of Redox Rich Diruthenium Compounds. *Inorg. Chem.* **2002**, *41*, 3521–3527.
- (41) Chisholm, M. H.; Clark, D. L.; Huffman, J. C.; Van der Sluys, W. G.; Kober, E. M.; Lichtenberger, D. L.; Bursten, B. E. The tungsten-tungsten triple bond. 13. Bisalkyl tetracarboxylates of dimolybdenum and ditungsten. Triple bonds between metal atoms with the valence molecular orbital description p⁴d². *J. Am. Chem. Soc.* 1987, 109, 6796–6816.
- (42) Hurst, S. K.; Xu, G. L.; Ren, T. Bis-adducts of substituted phenylethynyl on a Ru₂(DMBA)₄ core: Effect of donor/acceptor modifications. *Organometallics* **2003**, 22, 4118–4123.
- (43) Cordero, B.; Gomez, V.; Platero-Prats, A. E.; Reves, M.; Echeverria, J.; Cremades, E.; Barragan, F.; Alvarez, S. Covalent radii revisited. *Dalton Trans* **2008**, 2832–2838.
- (44) Lin, C.; Ren, T.; Valente, E. J.; Zubkowski, J. D. Synthesis, spectroscopy and electrochemistry of tetrakis(N,N'-diarylformamidinato)di(phenylethynyl)diruthenium(III). *J. Chem. Soc., Dalton Trans.* 1998, 571–576.
- (45) Pu, L.; Twamley, B.; Power, P. P. Synthesis and Characterization of 2,6-Trip $_2$ H $_3$ C $_6$ PbPbC $_6$ H $_3$ -2,6-Trip $_2$ (Trip $_2$ C $_6$ H $_2$ -2,4,6-i-Pr $_3$): A Stable Heavier Group 14 Element Analogue of an Alkyne. *J. Am. Chem. Soc.* **2000**, 122, 3524–3525.
- (46) Stender, M.; Phillips, A. D.; Wright, R. J.; Power, P. P. Synthesis and Characterization of a Digermanium Analogue of an Alkyne. *Angew. Chem., Int. Ed.* **2002**, *41*, 1785–1787.
- (47) Phillips, A. D.; Wright, R. J.; Olmstead, M. M.; Power, P. P. Synthesis and Characterization of 2,6-Dipp $_2$ -H $_3$ C $_6$ SnSnC $_6$ H $_3$ -2,6-Dipp $_2$ (Dipp = C_6 H $_3$ -2,6-Pr i_2): A Tin Analogue of an Alkyne. *J. Am. Chem. Soc.* **2002**, 124, 5930–5931.
- (48) Wright, R. J.; Phillips, A. D.; Hardman, N. J.; Power, P. P. The "Diindene" ArInInAr (Ar = C_6H_3 -2,6-Dipp₂, Dipp = C_6H_3 -2,6-Pri₂). Dimeric versus Monomeric In(I) Aryls: para-Substituent Effects in Terphenyl Ligands. *J. Am. Chem. Soc.* **2002**, *124*, 8538–8539.
- (49) Fischer, R. C.; Power, P. P. p-Bonding and the Lone Pair Effect in Multiple Bonds Involving Heavier Main Group Elements:

Developments in the New Millennium. Chem. Rev. 2010, 110, 3877—3923.

- (50) Lai, T. Y.; Tao, L.; Britt, R. D.; Power, P. P. Reversible Sn-Sn Triple Bond Dissociation in a Distannyne: Support for Charge Shift Bonding Character. *J. Am. Chem. Soc.* **2019**, *141*, 12527–12530.
- (51) Wedler, H. B.; Wendelboe, P.; Power, P. P. Second-Order Jahn-Teller (SOJT) Structural Distortions in Multiply Bonded Higher Main Group Compounds. *Organometallics* **2018**, *37*, 2929–2936.
- (52) Xu, G. L.; Jablonski, C. G.; Ren, T. $Ru_2(DMBA)_4(BF_4)_2$ and $Ru_2(DMBA)_4(NO_3)_2$: The first examples of diruthenium compounds containing BF_4^- and NO_3^- as ligands. *Inorg. Chim. Acta* **2003**, 343, 387–390.
- (53) Liu, I. P. C.; Ren, T. Density functional theory studies of structural deformation in bis(alkynyl) diruthenium(III): Stronger Ru-Ru bonding by any means necessary. *Inorg. Chem.* **2009**, *48*, 5608–561.
- (54) Becke, A. D. Density-functional exchange-energy approximation with correct asymptotic behavior. *Phys. Rev. A: At., Mol., Opt. Phys.* **1988**, 38, 3098–3100.
- (55) Becke, A. D. Density-functional thermochemistry. III. The role of exact exchange. *J. Chem. Phys.* **1993**, *98*, 5648–5652.
- (56) Vosko, S. H.; Wilk, L.; Nusair, M. Accurate spin-dependent electron liquid correlation energies for local spin density calculations: a critical analysis. *Can. J. Phys.* **1980**, *58*, 1200–1211.
- (57) Stephens, P. J.; Devlin, F. J.; Chabalowski, C. F.; Frisch, M. J. Ab Initio Calculation of Vibrational Absorption and Circular Dichroism Spectra Using Density Functional Force Fields. *J. Phys. Chem.* **1994**, *98*, 11623–11627.
- (58) Andrae, D.; Häußermann, U.; Dolg, M.; Stoll, H.; Preuß, H. Energy-adjusted ab initio pseudopotentials for the second and third row transition elements. *Theor. Chim. Acta* **1990**, *77*, 123–141.
- (59) Weigend, F.; Ahlrichs, R. Balanced basis sets of split valence, triple zeta valence and quadruple zeta valence quality for H to Rn: Design and assessment of accuracy. *Phys. Chem. Chem. Phys.* **2005**, *7*, 3297–3305.
- (60) Grimme, S.; Antony, J.; Ehrlich, S.; Krieg, H. A consistent and accurate ab initio parametrization of density functional dispersion correction (DFT-D) for the 94 elements H-Pu. *J. Chem. Phys.* **2010**, 132, 154104–154104.
- (61) Martin, R. L. Natural transition orbitals. J. Chem. Phys. 2003, 118, 4775–4777.
- (62) Apex3 v2016.9-0, Saint V8.34A, Saint V8.37A; Bruker AXS Inc.: Madison, WI, 2016.
- (63) SHELXTL suite of programs, Version 6.14; Bruker Advanced X-ray Solutions, Bruker AXS Inc., Madison, WI,, 2000–2003.
- (64) Sheldrick, G. M. In Acta Crystallogr., Sect. A: Found. Crystallogr. 2008; Vol. A64; pp 112–112.
- (65) Sheldrick, G. M. SHELXL 2016; University of Göttingen: Göttingen, Germany, 2016.
- (66) Sheldrick, G. M. Crystal structure refinement with SHELXL. Acta Crystallogr., Sect. C: Struct. Chem. 2015, 71, 3–8.